J Indian Acad Wood Sci
https://doi.org/10.1007/s13196-024-00344-3

ORIGINAL ARTICLE

Analysis of the density profile and bending properties of commercial particleboard

Hideaki Korai[1]

Received: 12 March 2024 / Accepted: 26 April 2024

Abstract This study comprehensively analyzed the bending properties of three types of commercial three-layer particleboards (Boards A, B, and C) to understand the intricate relationships between density profiles and bending properties. Density profiles notably varied among particleboards. Board A exhibited a heightened influence of the outer core-layer density on the bending properties, which surpasses that of the face-layer density. In contrast, Board C exhibited a greater influence of the face-layer density on the bending properties. Board B exhibited the same influence of the face-layer and outer core-layer densities on the bending properties. The outer core layers, manufactured with coarse particles retained long-wood fibers, thereby increasing the bending properties. The influence of the outer core layers on the bending properties varied among particleboards. The complexity in the mechanism of the bending properties was attributed to intricately intertwined factors: density, long-wood-fiber strength, and face-to-core ratio. In conclusion, this study highlights the multifaceted nature of bending properties, emphasizing the complexities among these factors.

Keywords Particleboard · Density profile · Bending properties · Wood fiber · Nondestructive test

✉ Hideaki Korai
korai@ffpri.affrc.go.jp

1 Forestry and Forest Products Research Institute, Tsukuba, Japan

Introduction

Previous studies (Korai 2022; Korai and Miyatake 2023) have shown that the outer core-layer density plays a more crucial role in increasing the bending properties of commercial particleboards than the face-layer density. This finding contradicts the conventional theory of bending properties, which asserts a direct proportionality between bending properties and face-layer density. In other words, according to the conventional theory, the bending properties of particleboards increase with an increase in face-layer density (Kawai and Sasaki 1986; Suo and Bowyer 1994; Wong et al. 1999, 2003). Generally, several studies on the bending properties of single-layer particleboards manufactured in laboratories have aligned with conventional theory, exhibiting an increase in bending properties with an increase in face-layer density. However, commercial particleboards have three layers (Gamage and Setunge 2015), which is markedly different from single-layer particleboards. As a result, their bending properties deviate from conventional theory (Korai 2022; Korai and Miyatake 2023). For the commercial particleboard, the core and face layers are manufactured with coarse and fine particles, respectively (Fig. 1) (Stark et al. 2010). Coarse particles retain long-wood fibers, whereas fine particles do not. The high bending properties are attributed to the coarse particles retaining long-wood fibers, whereas the fine particles fail to increase these properties because of the absence of long-wood fibers. Consequently, bending properties are primarily influenced by the outer core-layer density rather than the face-layer density (Korai 2022; Korai and Miyatake 2023). Benthien and Ohlmeyer (2017) investigated three-layer particleboards, but they focused on densification of face layers and did not investigate the effects of long-wood fibers on the bending properties. Shupin et al.

Published online: 24 June 2024

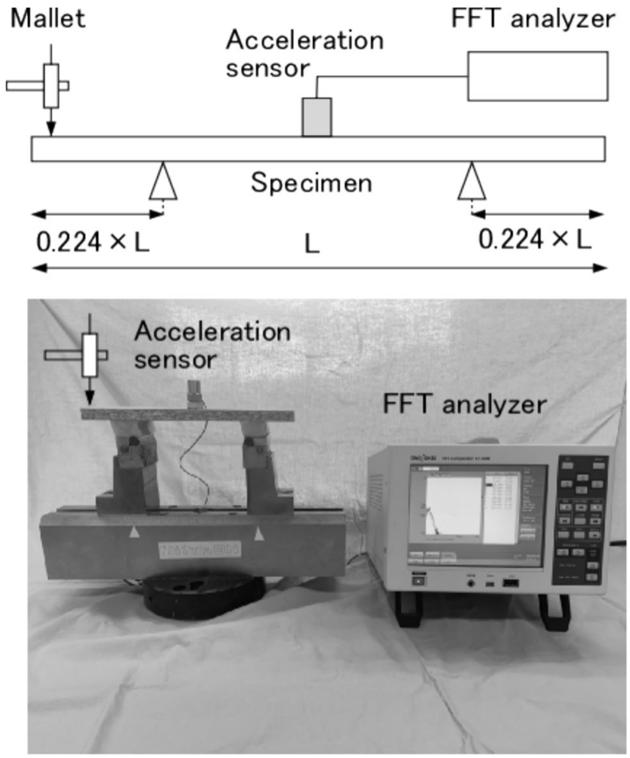

Fig. 1 Nondestructive bending vibration test using FFT analyzer. *Note*: FFT: fast Fourier transform. L is the length of the specimen (mm)

(2020) also investigated three-layer particleboards by altering the shape of the particles in the face layers. Their study suggested the importance of long-wood fibers. Reducing the density of particleboard is important (Benthien and Ohlmeyer 2017, 2018; Benthien et al. 2019), and effectively utilizing long-wood fibers may advance this reduction in density.

This finding of the previous studies (Korai 2022; Korai and Miyatake 2023) was derived from a type of particleboard manufactured in a factory (Factory A). To validate the reliability of this finding, two additional types of particleboard from different Japanese factories (Factories B and C) were analyzed. Additionally, the bending properties of these particleboards were investigated. It is worth noting that the bending properties encompass the modulus of rupture (MOR), static-bending Young's modulus (E_S), and dynamic bending Young's modulus. MOR and E_S were determined through a destructive test, specifically a static-bending test, whereas the dynamic bending Young's modulus was determined through a nondestructive test, specifically a bending vibration test (Fig. 1). The resultant modulus was defined as E_{BV}. Consequently, two Young's moduli (E_S and E_{BV}) were determined, and the relationships between the density of each layer and these moduli were analyzed. Furthermore, the relationships between E_{BV} and E_S, and between E_S (or E_{BV}) and MOR were analyzed.

Experimental

Bending test

Boards A, B, and C were manufactured in Japanese Factories A, B, and C, respectively. The core and face layers of particleboards were manufactured with coarse and fine particles, respectively. According to Japanese Industrial Standards (JIS) A 5908:2015 (JIS 2015), these particleboards were classified as type 18P. This standard was also employed to determine MOR and E_S. These particleboards had a thickness of 9.1 mm. Moreover, the densities of Boards A, B, and C were 0.784, 0.856, and 0.790 g/cm^3, respectively. Additionally, 70 specimens with dimensions of 50 mm × 210 mm were prepared from Boards B and C to investigate their bending properties. In a previous study (Korai and Miyatake 2023), 197 specimens of Board A were tested, resulting in 197 values with respect to bending properties. In this study, 70 values were randomly selected from this pool of 197 values for a comparative analysis of the bending properties of Boards B and C.

Nondestructive test

Nondestructive tests were conducted on the specimens before the static-bending test to investigate their bending properties using the bending-vibration test setup shown in Fig. 1. The signal obtained from the tests was amplified and transmitted to a fast Fourier transform (FFT) analyzer to determine the resonant frequency.

To calculate E_{BV}, free–free bending-vibration tests were conducted following the procedure outlined by Kubojima et al. (2017). The specimen was positioned on two small supports at the free–free vibration nodal positions (0.224 × L from each end) corresponding to its resonance mode. Subsequently, vibration was induced toward the thickness using a mallet at one end (Fig. 1). An acceleration sensor was used to detect the motion of the specimen at its midpoint. The obtained signal was processed using an FFT digital signal analyzer to extract high-resolution resonant frequencies. E_{BV} was then calculated based on the first-mode resonant frequency using the following equation:

$$E_{BV}(\mathrm{GPa}) = \frac{48\pi^2 L^4 F^2 \rho}{4.730^4 T^2} \times 10^{-12} \quad (1)$$

where L is the length of the specimen (mm), F is the first-mode resonant frequency (Hz), ρ is the specimen density (g/cm^3), and T is the specimen thickness (mm).

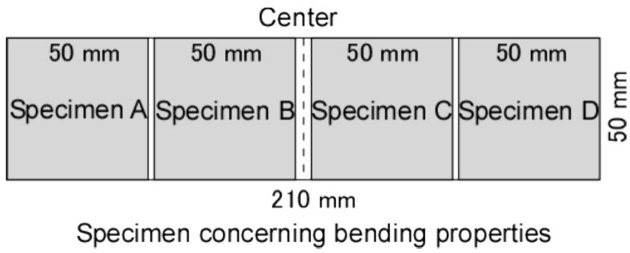

Fig. 2 Sampling positions of specimens A, B, C, and D for the density profile within the specimen concerning bending properties. *Note*: This is the top plane of the specimen

Density profile measurement

Figure 2 shows the sampling positions of Specimens A, B, C, and D for the density profile within the specimen with respect to bending properties. After the static-bending test, two adjacent density profile specimens (Specimens B and C), each measuring 50 mm × 50 mm, were derived from one bending-property specimen. A previous study (Korai and Miyatake 2023) showed that Specimens A and D were ineffective in predicting bending properties. As a result, these specimens were excluded from this study. Specimens B and C were scanned using a density profile measurement system, specifically an X-ray densitometer (DA-X 6000, GreCon, Germany). A digital microscope (VHX-8000, KEYENCE, Japan) was used to measure the thickness of the face layers. Figure 3 shows the definition of each layer (L1–L9) and the gross densities in the density profile. The density was measured at intervals of 0.1 mm along the specimen thickness, and the mean density of each layer was calculated. For instance, L1 density was determined by averaging the measurements taken at thicknesses of 0.2–0.7 mm and 8.4–8.9 mm.

Results and discussion

Density profile

Figure 3 shows the density profiles of Boards A, B, and C. The face layers (L1–L3) of Boards A and C were manufactured with fine particles, whereas the core layers (L4–L9) were manufactured with coarse particles. L4 denotes the outer core layers of Boards A and C. For Board B, the face layers (L1–L4) were manufactured with fine particles, whereas the core layers (L5–L9) were manufactured with coarse particles. L5 denotes the outer core layers of Board B. Notably, the outer core layers of Board B were positioned more internally than those of Boards A and C.

The density profiles of Boards A, B, and C exhibited distinct shapes. Tables 1, 2 and 3 show the mean density of each layer of Boards A, B, and C, respectively. The L1 density of Boards B and C was higher than that of Board A. Notably, the L1 of Board A has a round shape, while those of Boards B and C have a pointed shape. Additionally, the core layer of Board A appears flat, contrasting the steep shape observed in Boards B and C. However, the formation of these density profiles remains unclear, and diverse

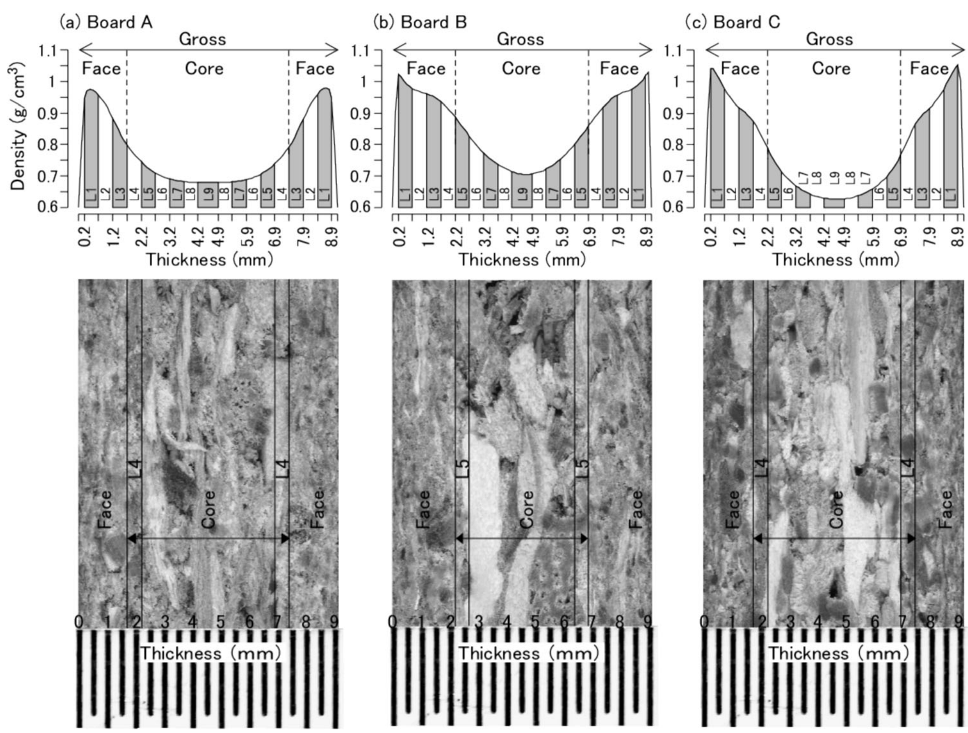

Fig. 3 Definition of layers 1–9 (L1–L9) and gross densities in the density profile. *Note*: This is the through-layer thickness plane of the density profile specimens. Boards A, B, and C were manufactured in Japanese Factories A, B, and C, respectively

Table 1 Mean, SD, CV, maximum, minimum, and range for the density of each layer on Board A

	L1	L2	L3	L4	L5	L6	L7	L8	L9	Gross
Mean (g/cm^3)	0.966	0.925	0.839	0.769	0.724	0.699	0.689	0.684	0.684	0.784
SD (g/cm^3)	0.012	0.011	0.010	0.013	0.013	0.011	0.012	0.014	0.015	0.008
CV (%)	1.24	1.19	1.19	1.69	1.80	1.57	1.74	2.05	2.19	1.02
Maximum (g/cm^3)	1.01	0.948	0.861	0.795	0.752	0.720	0.716	0.708	0.710	0.801
Minimum (g/cm^3)	0.935	0.899	0.808	0.726	0.679	0.670	0.658	0.647	0.643	0.757
Range (g/cm^3)	0.08	0.049	0.053	0.069	0.073	0.050	0.058	0.061	0.067	0.044

SD standard deviation, *CV* coefficient of variation, Range was difference between maximum and minimum values. See Fig. 3 for L1–L9 and gross. Board A was manufactured in Japanese Factory A

Table 2 Mean, SD, CV, maximum, minimum, and range for the density of each layer on Board B

	L1	L2	L3	L4	L5	L6	L7	L8	L9	Gross
Mean (g/cm^3)	0.999	0.970	0.947	0.904	0.848	0.792	0.751	0.725	0.714	0.856
SD (g/cm^3)	0.038	0.043	0.043	0.043	0.043	0.043	0.042	0.042	0.043	0.040
CV (%)	3.80	4.43	4.54	4.76	5.07	5.43	5.59	5.79	6.02	4.67
Maximum (g/cm^3)	1.09	1.08	1.05	1.01	0.956	0.895	0.855	0.832	0.813	0.956
Minimum (g/cm^3)	0.925	0.890	0.854	0.811	0.762	0.716	0.672	0.646	0.639	0.781
Range (g/cm^3)	0.17	0.19	0.20	0.20	0.194	0.179	0.183	0.186	0.174	0.175

SD standard deviation. *CV* coefficient of variation. Range was difference between maximum and minimum values. See Fig. 3 for L1–L9 and gross. Board B was manufactured in Japanese Factory B

Table 3 Mean, SD, CV, maximum, minimum, and range for the density of each layer on Board C

	L1	L2	L3	L4	L5	L6	L7	L8	L9	Gross
Mean (g/cm^3)	1.02	0.946	0.899	0.830	0.744	0.688	0.655	0.637	0.631	0.790
SD (g/cm^3)	0.038	0.037	0.033	0.032	0.029	0.027	0.025	0.025	0.025	0.028
CV (%)	3.74	3.91	3.67	3.86	3.90	3.92	3.82	3.92	3.96	3.54
Maximum (g/cm^3)	1.12	1.05	0.974	0.902	0.813	0.761	0.720	0.703	0.694	0.859
Minimum (g/cm^3)	0.955	0.885	0.841	0.768	0.699	0.651	0.621	0.603	0.595	0.748
Range (g/cm^3)	0.17	0.17	0.133	0.134	0.114	0.110	0.099	0.100	0.099	0.111

SD standard deviation. *CV* coefficient of variation. Range was difference between maximum and minimum values. See Fig. 3 for L1–L9 and gross. Board C was manufactured in Japanese Factory C

shapes may introduce complexity to the mechanism of the bending properties.

Histogram of the bending properties

Figure 4 shows the MOR histograms for Boards A, B, and C. Although MOR typically follows a normal distribution, the distributions shown in Fig. 4 exhibit a distinct trend. Similar to the density profiles, the MOR histograms of Boards A, B, and C exhibit variations. Figures 5 and 6 show the histograms of E_S and E_{BV}, respectively. These histograms also exhibit variations, potentially posing challenges in analyzing the mechanism of the bending properties.

Correlation coefficient between each layer density and MOR

Tables 1, 2 and 3 show the standard deviation, coefficient of variation (CV), maximum, minimum, and range (maximum–minimum) for the density of each layer on Boards A, B, and C. Board A exhibited a lower CV than Boards B and C, and its range was narrower than those of Boards B and C. Essentially, the density variation of Board A was less pronounced than that of Boards B and C. Lower and

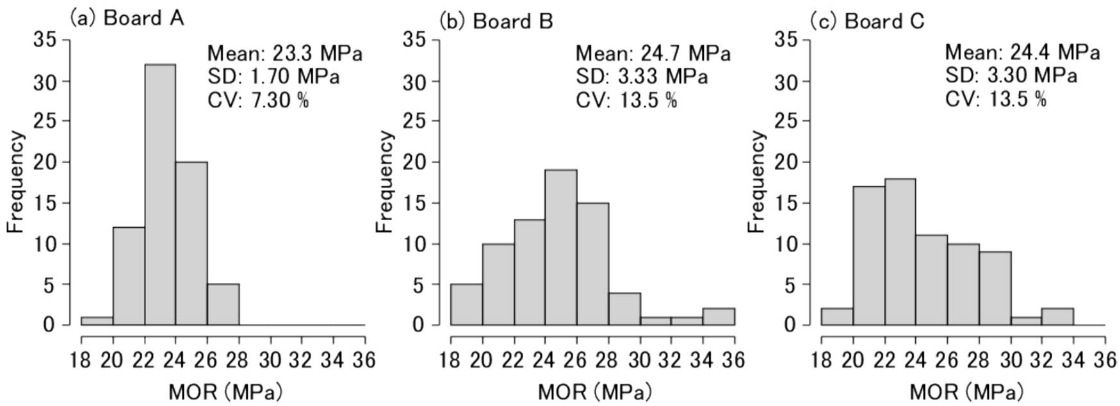

Fig. 4 MOR histogram of Boards A, B, and C. Note: MOR: modulus of rupture, SD: standard deviation, CV: coefficients of variation, Sample size was 70. Boards A, B, and C were manufactured in Japanese Factories A, B, and C, respectively

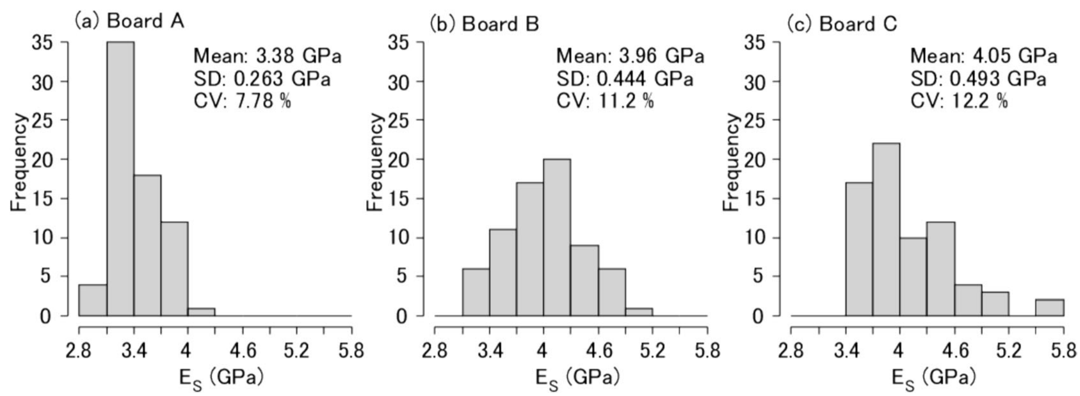

Fig. 5 E_S histogram of Boards A, B, and C. Note: E_S: static bending Young's modulus, SD: standard deviation, CV: coefficients of variation, Sample size was 70. Boards A, B, and C were manufactured in Japanese Factories A, B, and C, respectively

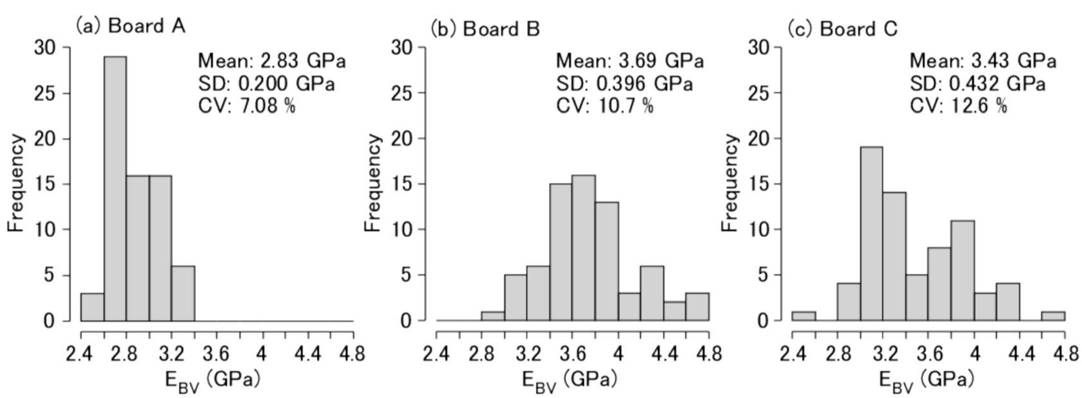

Fig. 6 E_{BV} histogram of Boards A, B, and C. Note: E_{BV}: dynamic bending Young's modulus by bending vibration test, SD: standard deviation, CV: coefficients of variation, Sample size was 70. Boards A, B, and C were manufactured in Japanese Factories A, B, and C, respectively

higher density variations correspond to lower and higher bending-property variations, respectively.

Table 4 shows the correlation coefficients between the density of each layer and MOR for Boards A, B, and C. A subset of these results is shown in Fig. 7 as examples. The correlation coefficients of Board A were lower than those of Boards B and C. Low variations in density and MOR on Board A led to overfitting, resulting in a lower correlation coefficient. In contrast, high variations in density and MOR

Table 4 Correlation coefficients between the density of each layer and the MOR on Boards A, B, and C

	L1	L2	L3	L4	L5	L6	L7	L8	L9	Gross
Board A	0.100	0.082	0.330	0.614	0.618	0.560	0.216	0.015	− 0.095	0.381
Board B	0.639	0.599	0.605	0.620	0.623	0.580	0.541	0.491	0.418	0.595
Board C	0.786	0.759	0.721	0.689	0.666	0.622	0.626	0.634	0.603	0.725

MOR modulus of rupture. See Fig. 3 for L1–L9 and gross. Boards A, B, and C were manufactured in Japanese Factories A, B, and C, respectively

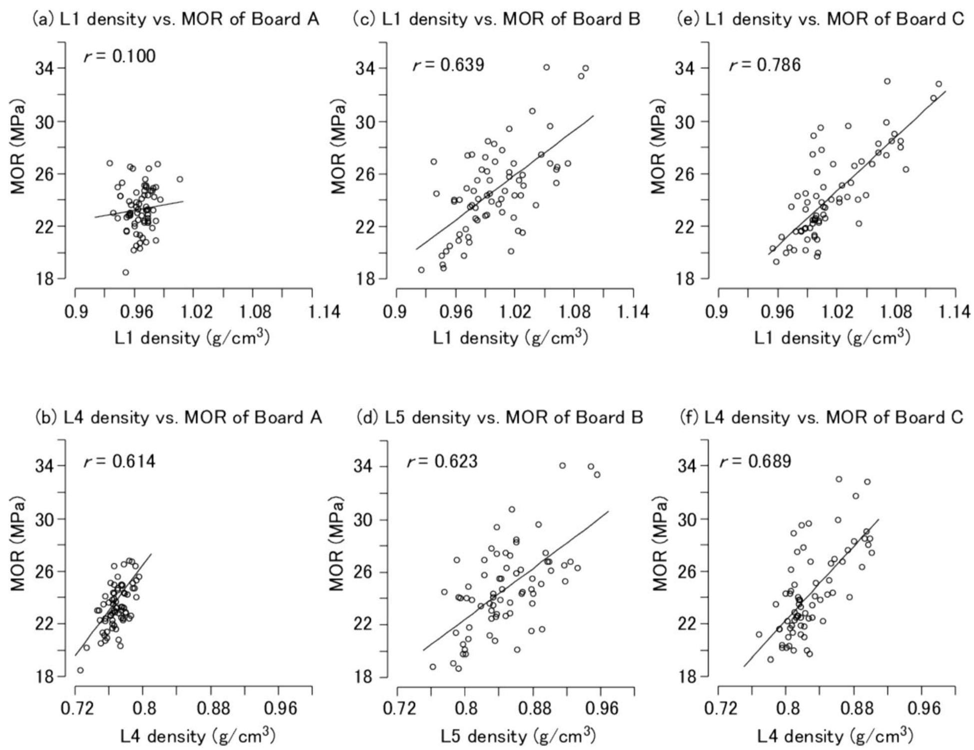

Fig. 7 **a** Relationship between L1 density and MOR of Board A, **b** relationship between L4 density and MOR of Board A, **c** relationship between L1 density and MOR of Board B, **d** relationship between L5 density and MOR of Board B, **e** relationship between L1 density and MOR of Board C, **f** relationship between L4 density and MOR of Board C. Note: MOR: modulus of rupture, *r*: correlation coefficient, See Fig. 3 for L1, L4, and L5 densities. Boards A, B, and C were manufactured in Japanese Factories A, B, and C, respectively

Table 5 Correlation coefficients between the density of each layer and the Es on Boards A, B, and C

	L1	L2	L3	L4	L5	L6	L7	L8	L9	Gross
Board A	0.362	− 0.009	0.150	0.491	0.504	0.458	0.120	− 0.095	− 0.186	0.315
Board B	0.717	0.699	0.710	0.718	0.697	0.660	0.645	0.622	0.594	0.700
Board C	0.704	0.690	0.655	0.605	0.569	0.553	0.581	0.597	0.550	0.655

E_S static bending Young's modulus. See Fig. 3 for L1–L9 and gross. Boards A, B, and C were manufactured in Japanese Factories A, B, and C, respectively

on Boards B and C prevented overfitting, yielding higher correlation coefficients.

Complexity of the mechanism of the bending properties

Theoretically, an increase in face-layer density increases the MOR (Kawai and Sasaki 1986; Suo and Bowyer 1994; Wong et al. 1999, 2003). However, this theory may not be

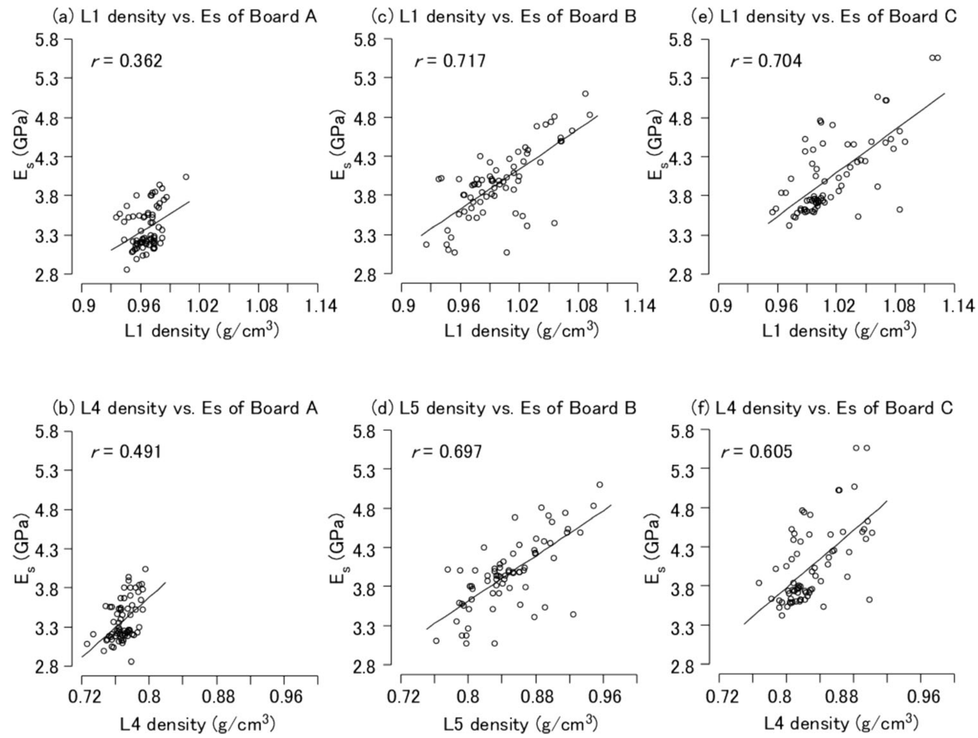

Fig. 8 **a** Relationship between L1 density and E_S of Board A, **b** relationship between L4 density and E_S of Board A, **c** relationship between L1 density and E_S of Board B, **d** relationship between L5 density and E_S MOR of Board B, **e** relationship between L1 density and E_S of Board C, **f** relationship between L4 density and E_S of Board C. Note: E_S: static bending Young's modulus, *r*: correlation coefficient, See Fig. 3 for L1, L4, and L5 densities. Boards A, B, and C were manufactured in Japanese Factories A, B, and C, respectively

Table 6 Correlation coefficients between the density of each layer and the E_{BV} on Boards A, B, and C

	L1	L2	L3	L4	L5	L6	L7	L8	L9	Gross
Board A	0.247	0.075	0.286	0.567	0.576	0.538	0.194	− 0.009	− 0.111	0.411
Board B	0.930	0.938	0.926	0.917	0.898	0.888	0.870	0.860	0.836	0.929
Board C	0.758	0.755	0.714	0.675	0.655	0.628	0.640	0.657	0.614	0.721

E_{BV} dynamic Young's moduli by bending vibration test. See Fig. 3 for L1–L9 and gross. Boards A, B, and C were manufactured in Japanese Factories A, B, and C, respectively

applicable to commercial particleboards, which typically have three layers. The face layers manufactured with fine particles lacking long-wood fibers did not exhibit an increase in strength. In contrast, the core layer manufactured with coarse particles retaining long-wood fibers exhibits an increase in strength (Korai 2022; Korai and Miyatake 2023). Contrary to theoretical expectations, the MOR of a three-layer particleboard is not expected to be influenced by the face-layer density because of the absence of long-wood fibers in the fine particles of the face layers (Korai 2022; Korai and Miyatake 2023). Consequently, coarse particles in L4 increased MOR, whereas fine particles in L1 did not induce such changes. As a result, the correlation coefficient of L4 was higher than that of L1, and the MOR did not increase with an increase in L1 density.

The outer core layers of Board B were positioned more internally than those of Board A (Fig. 3). Specifically, the outer core layer of Board B was identified as L5, not L4. For Board B, the significance of L5 might outweigh that of L4. Instead of comparing the correlation coefficients of L1 and L4, the correlation coefficients of L1 and L5 were investigated, and the results revealed their near equivalence (Table 4). Although the density of L5 in Board B (0.848 g/cm^3, Table 2) surpassed that of L4 in Board A (0.769 g/cm^3, Table 1), the effectiveness of L5 in increasing MOR was limited because it is positioned more internally than L4.

The outer core layers of Board C were identical to those of Board A and were identified as L4. However, unlike Board A, the correlation coefficient of L1 was higher than that of L4 on Board C. This difference can be attributed to the considerably higher L1 density on Board C (1.015 g/cm^3, Table 3) than on Board A (0.966 g/cm^3, Table 1); 1.015 g/cm^3 is notably high. Therefore, it may be influenced by the face-layer density, following conventional theory (Benthien and Ohlmeyer 2017). For Board C, the positive impact of the high L1 density outweighs the negative impact of fine particles lacking long-wood fibers, resulting in a higher correlation coefficient for L1 than L4.

The layer density, strength of long-wood fibers, and internal position of the outer core layer (face-to-core ratio)

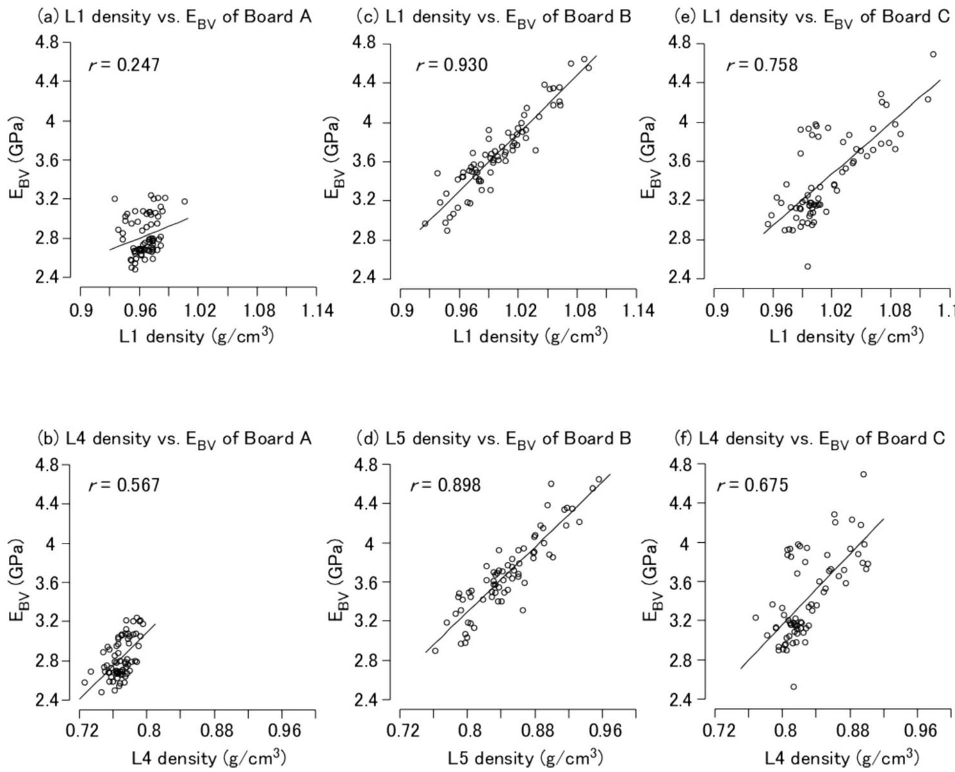

Fig. 9 **a** Relationship between L1 density and E_{BV} of Board A, **b** relationship between L4 density and E_{BV} of Board A, **c** relationship between L1 density and E_{BV} of Board B, **d** relationship between L5 density and E_{BV} of Board B, **e** relationship between L1 density and E_{BV} of Board C, **f** relationship between L4 density and E_{BV} of Board C. Note: E_{BV}: dynamic bending Young's modulus by bending vibration test, *r*: correlation coefficient, See Fig. 3 for L1, L4, and L5 densities. Boards A, B, and C were manufactured in Japanese Factories A, B, and C, respectively

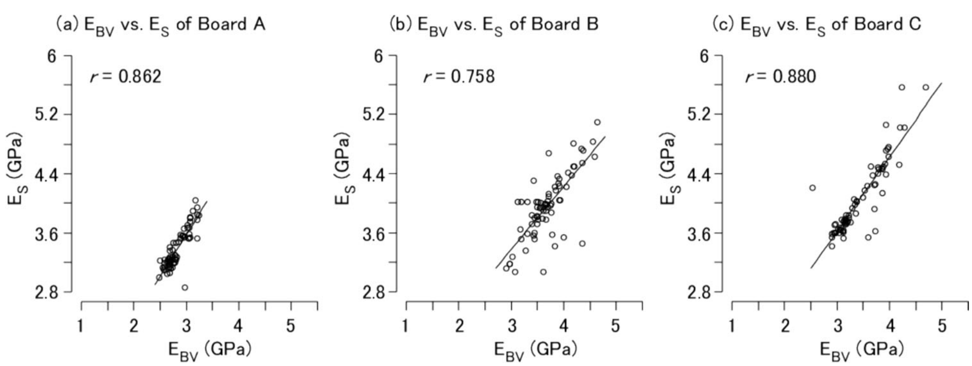

Fig. 10 **a** Relationship between E_{BV} and E_S of Board A, **b** relationship between E_{BV} and E_S of Board B, **c** relationship between E_{BV} and E_S of Board C, Note: E_S: static bending Young's modulus, E_{BV}: dynamic bending Young's modulus by bending vibration test, *r*: correlation coefficient, Boards A, B, and C were manufactured in Japanese Factories A, B, and C, respectively

are intricately intertwined, contributing to the complexity of the MOR mechanism. In terms of particleboard manufacturing, achieving a high L1 density, as in Board C, is challenging. To increase MOR, the thickness of the face layers must be reduced to efficiently utilize the long-wood fibers in the outer core layers. Ideally, face layers should be as thin as possible or even excluded.

Relationship between dynamic- and static-bending Young's moduli

Table 5 shows the correlation coefficients between the density of each layer and E_S on Boards A, B, and C. A subset of these results is shown in Fig. 8 as examples. The observed trend aligns with that of MOR. Specifically, for Board A, the correlation coefficient of L4 surpassed that of L1. For Board B, the correlation coefficients for L1 and L5 are similar. Meanwhile, for Board C, the correlation coefficient of L1 exceeded that of L4. Table 6 shows the

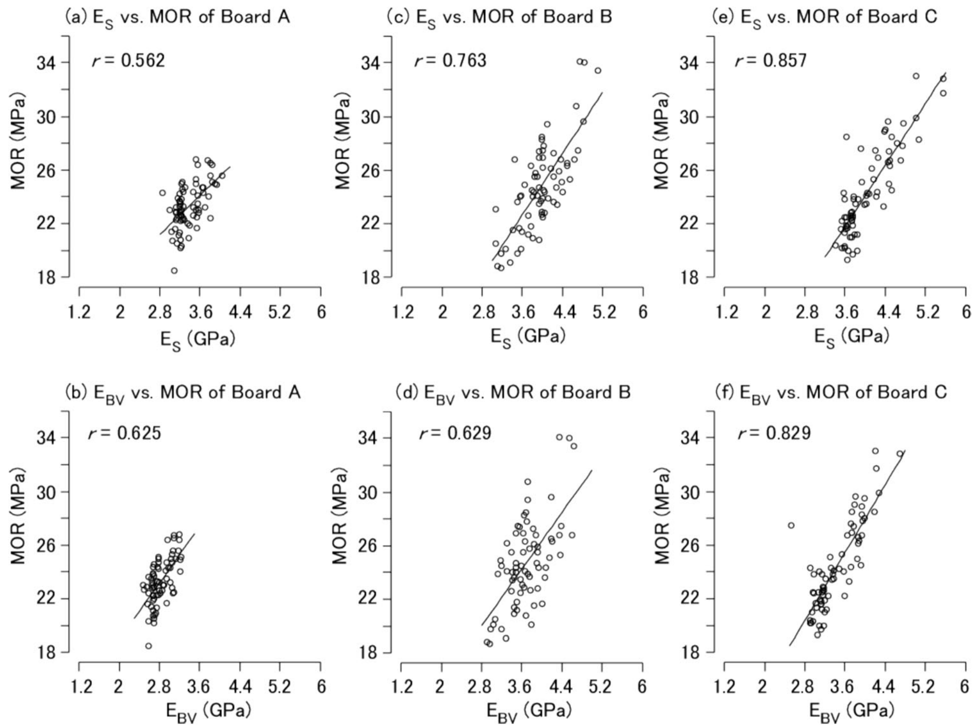

Fig. 11 **a** Relationship between E_S and MOR of Board A, **b** relationship between E_{BV} and MOR of Board A, **c** relationship between E_S and MOR of Board B, **d** relationship between E_{BV} and MOR of Board B, **e** relationship between E_S and MOR of Board C, **f** relationship between E_{BV} and MOR of Board C. Note: MOR: modulus of rupture, E_S: static bending Young's modulus, E_{BV}: dynamic bending Young's modulus by bending vibration test, *r*: correlation coefficient, Boards A, B, and C were manufactured in Japanese Factories A, B, and C, respectively

correlation coefficients between the density of each layer and E_{BV} on Boards A, B, and C. A subset of these results is shown in Fig. 9 as examples. This trend mirrors that observed for MOR and E_S, and the complexity of E_S and E_{BV} mechanisms is also exhibited.

In this study, two bending Young's moduli, E_S and E_{BV} were determined. Additionally, it is crucial to develop a predictive model for E_S obtained through a destructive test, using E_{BV} obtained through a nondestructive test. Figure 10 shows the relationship between E_{BV} and E_S for Boards A, B, and C. The notably high correlation coefficients between E_{BV} and E_S suggest the suitability of E_{BV} for predicting E_S. Determining E_{BV} is a straightforward process involving, which involves measuring the first-mode resonant frequency and substituting it into Eq. (1). Despite the narrow density range of Board A (Table 1), which may be susceptible to overfitting, the high correlation coefficients between E_{BV} and E_S (Fig. 10a) indicate that E_S can be reliably predicted using this nondestructive test.

Relationship between dynamic-bending Young's moduli and MOR

According to previous studies (Jin et al. 2009; Wei et al. 2013; Kojima et al. 2016), there is usually a high correlation between bending Young's modulus and MOR. However, these experiments involved manufacturing particleboards with a wide range of densities to investigate the relationship between the bending Young's modulus and MOR. The inclusion of a wide density range effectively prevented overfitting and exhibited a high correlation between the bending Young's modulus and MOR. In contrast, this study revealed that achieving wide-range densities is impractical for commercial particleboards, making overfitting highly probable. Moreover, the shape of the MOR histogram differed from that of each bending Young's modulus. This suggests that the correlation between bending Young's modulus and MOR may not be high. Therefore, the relationships between the bending Young's modulus and MOR were investigated (Fig. 11). Furthermore, this study demonstrated that E_S (or E_{BV}) and MOR are indeed correlated but to a lesser extent than is commonly assumed, particularly when Board A has low correlation coefficients. Unlike laboratory particleboards, this study experienced overfitting owing to the limited density range of commercial particleboards. Therefore, commercial particleboards do not exhibit a higher correlation between bending Young's moduli and MOR than is generally presumed. Unlike E_S (Fig. 10), MOR may not be reliably predicted through a nondestructive test.

Conclusions

The mechanism of bending properties is complex, involving factors such as density, strength of long-wood fibers, and face-to-core ratio, all of which are intricately intertwined. Therefore, it is essential to determine the optimal manufacturing conditions to increase the bending properties of particleboards. Specifically, to efficiently utilize outer core layers containing long-wood fibers, it is necessary to minimize the thickness of the face layers—ideally as thin as possible. For structural applications, face layers may be considered unnecessary. A single-layer particleboard manufactured exclusively with coarse particles is superior to a three-layer particleboard. Although E_S can be reliably predicted using this nondestructive test, MOR prediction may present an interesting challenge.

Acknowledgements The author expresses gratitude to the three Japanese factories for providing the particleboards and to Mr. Kenta Endo of KEYENCE CORPORATION for photographing the cross-section of the particleboards and measuring the thicknesses of the face layers. The author also expresses gratitude to Mr. Atsushi Miyatake of the Forestry and Forest Products Research Institute for his kind advice.

References

Benthien JT, Ohlmeyer M (2017) Influence of face to core ratio and core layer resin content on the properties of density-decreased particleboard. Eur J Wood Prod 75:55–62

Benthien JT, Ohlmeyer M (2018) Enhancement of low-density particleboard properties by core layer particle orientation. Eur J Wood Prod 76:1087–1091

Benthien JT, Ohlmeyer M (2019) Effect of increasing core layer particle thickness on lightweight particleboard properties. Eur J Wood Prod 77:1029–1043

Gamage N, Setunge S (2015) Modelling of vertical density profile of particleboard, manufactured from hardwood sawmill residue. Wood Mat Sci Eng 10:157–167

Japanese Industrial Standards (2015) JIS standard specification for particleboard. JIS A 5908. Japanese Standards Association, Tokyo

Jin J, Dai C, Hsu E, Yu C (2009) Properties of strand boards with uniform and conventional vertical density profiles. Wood Sci Technol 43:559–574

Kawai S, Sasaki H (1986) Production technology for low-density particleboard I. Forming a density gradient and its effect on board properties. Mokuzai Gakkaishi 32:324–330

Kojima Y, Sakakibara A, Kobori H, Suzuki S (2016) Evaluating the durability of wood-based panels by a non-destructive bending test. J Wood Sci 62:263–269

Korai H (2022) Effects of density profile on bending strength of commercial particleboard. Forest Prod J 72:85–92

Korai H, Miyatake A (2023) Effect of outer core-layer density on bendingproperties of commercial particleboard. Wood Mat Sci Eng 18(3):943–951

Kubojima Y, Tonosaki M (2012) Young's and shear moduli of glued laminated timber composed of different species obtained by a flexural vibration test. Holzforschung 66:871–875

Kubojima Y, Suzuki Y, Kato H, Kobayashi I (2017) Parabolic behavior of the Young's moduli ratio of wood obtained by vibration tests with time during drying. Wood and Fiber Sci 49:260–268

Kubojima Y, Sonoda S, Kato H, Harada M (2020) Effect of shear and rotatory inertia on the bending vibration method without weighing specimens. J Wood Sci. https://doi.org/10.1186/s10086-020-01900-4

Shupin L, Li G, Wenjing G (2020) Effect of face layer manipulation on the density profile and properties of low density particleboard. Wood Res 65:125–134

Stark NM, Cai Z, Carll C (2010) Wood-Based Composite Materials Panel Products, Glued-Laminated Timber, Structural Composite Lumber, and Wood–Nonwood Composite Materials. Wood handbook. Chapter 11 p11 Madison: USDA Forest Service

Suo S, Bowyer JL (1994) Simulation modeling of particleboard density profile. Wood Fiber Sci 26:397–411

Wei L, Jia Y, Xiangdong L, Lili M, Yuhua W (2013) Nondestructive testing and performance prediction of soybean stalk board. BioResources 8:4797–4804

Wong ED, Zhang M, Wang Q, Kawai S (1999) Formation of density profile and its effects on properties of particleboard. Wood Sci Tech 33:327–340

Wong ED, Yang P, Zhang M, Wang Q, Nakao T, Li KF, Kawai S (2003) Analysis of the effects of density profile on the bending properties of particleboard using finite element method (FEM). Holz Als Roh- und Werkstoff 61:66–72